Supporting Material

Diurnal and day-to-day characteristics of ambient particle mass size distributions from HR-ToF-AMS measurements at an urban site and a suburban site in Hong Kong

Berto P. Lee[1], Hao Wang[2], and Chak K. Chan[1,2*]

[1]School of Energy and Environment, City University of Hong Kong, Hong Kong, China

[2]Division of Environment, Hong Kong University of Science and Technology, Hong Kong, China

Correspondence to: Chak K. Chan (chak.k.chan@cityu.edu.hk)

A. Particle size characterization by HR-AMS

The working principle of the AMS has been described extensively in the literature [*Canagaratna et al.*, 2007; *DeCarlo et al.*, 2006; *Drewnick et al.*, 2005; *Jimenez et al.*, 2003; *Jimenez et al.*, 2007]. The particle size acquisition mode (*PToF mode*) relies on aerodynamic sizing as the measurement of particle flight time between two fixed points in space in near vacuum conditions. The incident particle beam passes a rotating double-slitted disk, which permits pulses of particles to enter the flight chamber. The chopper operates at a fixed frequency (150 Hz) and has a duty cycle of 2-4% depending on individual instruments. The acceleration of a particle into the vacuum interior of the AMS is a function of its size [*Jimenez et al.*, 2003] and thus particles of different size in the pulse ensemble travel at different velocities which are determined from particle flight times over a fixed flight path (i.e. the length of the chamber). Ions arriving at the detector are counted as a function of time between two subsequent particle packages passing through the particle chopper slit. Averaging over several chopper cycles yields a distribution of ions with respect to particle size and enables the measurement of mass concentrations of specific ions as a function of particle size, or of specific bulk species (Organics, SO4, NO3, NH4, Chl) by employing the fragmentation table as in the unit mass resolution acquisition mode (*V-mode*). In contrast to V-mode, where particle contributions to measured ion mass are inferred from the difference of blocked and unblocked particle beam spectra, the baseline for integration in the PToF mode is established by the averaging of two defined time regions (*DC markers*) at the very beginning and the very end of a chopper cycle which correspond to velocities of particle sizes beyond the transmission capability of the aerodynamic lens inlet assembly and can thus represent signal background contributions. The primary logged information in PToF mode is the particle flight time from which velocity is inferred due to the fixed length of the flight path. Each velocity can be associated with a particle of certain vacuum aerodynamic diameter by calibration with a set of particles of known size. The relationship between geometric (D_p) and vacuum-aerodynamic diameter (D_{va}) is as follows [*Jayne et al.*, 2000]:

$$D_{va} = D_p \times \delta_p \times S \qquad Eq.\ A1$$

where δ_p is the particle density and S a particle shape factor for particles that are non-spherical or have internal voids. S has been experimentally determined for nitrate (S=0.8). For most other particles, especially particle mixtures, S is commonly ignored, i.e. particles are assumed spherical with S=1. A more fundamental discussion of the relationships of different particle diameters and their relation to particle density has been provided elsewhere [*DeCarlo et al.*, 2004; *Slowik et al.*, 2004]. For the particle size calibration, a set of monodisperse polystyrene latex particles (PSL, Duke Scientific, CA) in the range of 80nm to 800nm was used in this study. As PSL does not vaporize fast enough at 600°C, the vaporizer temperature is temporarily increased to 800°C. To compensate for the slow evaporation of larger sized PSL particles with relatively broad time-of-flight peaks, the sum of leading edge flight time and one half of the chopper width (*0.5*duty cycle/chopper frequency*) is chosen to approximate PSL particle flight time. Particle velocity is determined from the chamber flight length (0.295m for the HR-AMS) and the flight time as measured using the above procedure. D_{va} in nm and particle velocity v in m/s are related empirically by the following equation [*Jayne et al.*, 2000]:

$$v = v_l + \frac{v_g - v_l}{1 + \left(\frac{D_{va}}{D^*}\right)^b} \qquad Eq.\ A2$$

where v_l is the gas velocity inside the aerodynamic lens, v_g the velocity of the gas as it leaves the lens, D_{va} the vacuum aerodynamic diameter calculated from the PSL particle diameter and the PSL density of 1.05 g/cm³ and a shape factor of 1. D* and b are empirical parameters without concrete physical meaning. As per calibration only particle velocity v and vacuum aerodynamic diameter D_{va} are known. The remaining parameters are determined by a non-linear curve fit of v against D_{va} using the above relationship.

B. Lognormal peak fitting

Lognormal peaks were fitted to the original AMS mass size distributions employing the *Multipeak Fit V2* algorithm in *Igor Pro (Wavemetrics)* using a simple vertical offset as the baseline and initial guesses on peak position, height, and width based on visual inspection of the raw size distribution. The peak fitting algorithm iteratively adjusts the initial fit with the objective of minimizing fit residuals (*i.e. the difference of original and reconstructed distributions*) in the final solution. In cases where excessive deviations from the initial guesses were evident, e.g. greatly shifted peak locations and large changes in peak shape (especially large fluctuations in peak width), fitting parameters from immediately adjacent size distributions (i.e. the previous and next distribution in sequence) were used to adjust the fitting process by fixing either the location (*primary*) or the width of the peak (*secondary*) to the average value of the adjacent fitted distributions. To evaluate longer term trends in size distributions, the raw 10min size distributions were averaged to yield 24h size distributions (covering the time period from 00:00 to 23:59 each day), enabling the evaluation of progressive changes in particle size distributins in each season. To examine regular reoccuring trends, diurnal variations in size distributions were evaluated. For this purpose, size distributions aquired within the same hour of day were grouped for each continous sampling season at both measurement sites. Establishing diurnal trends generally involves the averaging of measurement data from vastly different concentraton regimes within each

continous measurement period, and the averaging of mass (or volume) based size distribution involves different uncertainties for each size bin, mainly due to the cubic relationship between particle mass (or volume) and particle diameter. Correspondingly, the signal to noise ratio improves greatly for size bins towards to the upper end of the range covered by the AMS. In order to establish reliable diurnal trends, we evaluated size distributions reconstructed from the average, median, 25th and 75th percentile of each size bin. Similar diurnal trends in the fitting parameters across these different size distributions would confirm that changes were indeed recurrent on a daily basis while divergent trends would indicate that irregular processes (e.g. episodic events) were more significant in determining size distribution characteristics. Since episodic pollution events and clean periods (e.g prolonged precipitation) were not removed from the dataset, the quantitative analysis focuses on trends observed in the median dataset to minimize skewing effects of high and low concentration periods.

C. Additional Tables

Table C1. Median organic subcomponent concentrations in NR-PM$_1$ prior to and during meal hours at the urban MK site and their fractional contribution to total change in Organics in NR-PM$_1$ [*Lee et al.*, 2015]

Mass conc. μg m^{-3}	SOA	COA	HOA	Total Org		SOA	COA	HOA	Total Org	
Pre lunch (09:00 – 11:00)	3.9	3.0	3.9	10.9		1.6	2.6	2.3	6.5	
Lunch (12:00 – 14:00)	4.6	7.0	4.0	15.8	Spring	1.8	4.0	2.1	8.0	Summer
% of Total Org change	+16.3%	+81.4%	+2.3%			+18.3%	+94.1%	-8.6%		
Pre dinner (15:00 – 17:00)	4.4	4.0	3.8	12.1		1.7	3.3	2.3	7.3	
Dinner (19:00 – 21:00)	4.6	9.2	4.1	17.9		1.6	6.3	2.3	10.1	
% of Total Org change	+4.7%	+89.6%	+5.7%			-4.4%	+106.3%	-1.9%		

Table C2. Ratio of 10th and 90th percentile mass concentration to median mass concentration of submicron (NR-PM$_1$) species at the the urban MK site [*Lee et al.*, 2015]

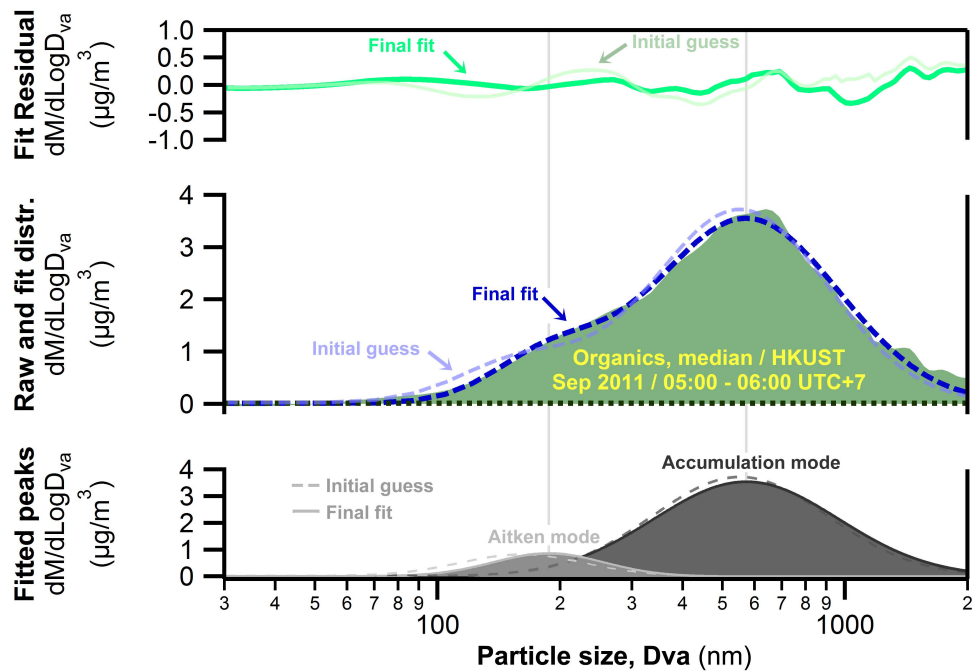| PC ratio	Org	SO4	NO3	
PC10 / PC50	0.5	0.3	0.3	Spring
PC90 / PC50	2.1	1.7	2.8	
PC10 / PC50	0.4	0.3	0.5	Summer
PC90 / PC50	2.3	1.8	2.2	

D. Additional Figures

Figure D1. Example of a log-normal peak fit *(Multipeak Fit V2, Igor Pro, Wavemetrics)* of an AMS organic-species size distribution
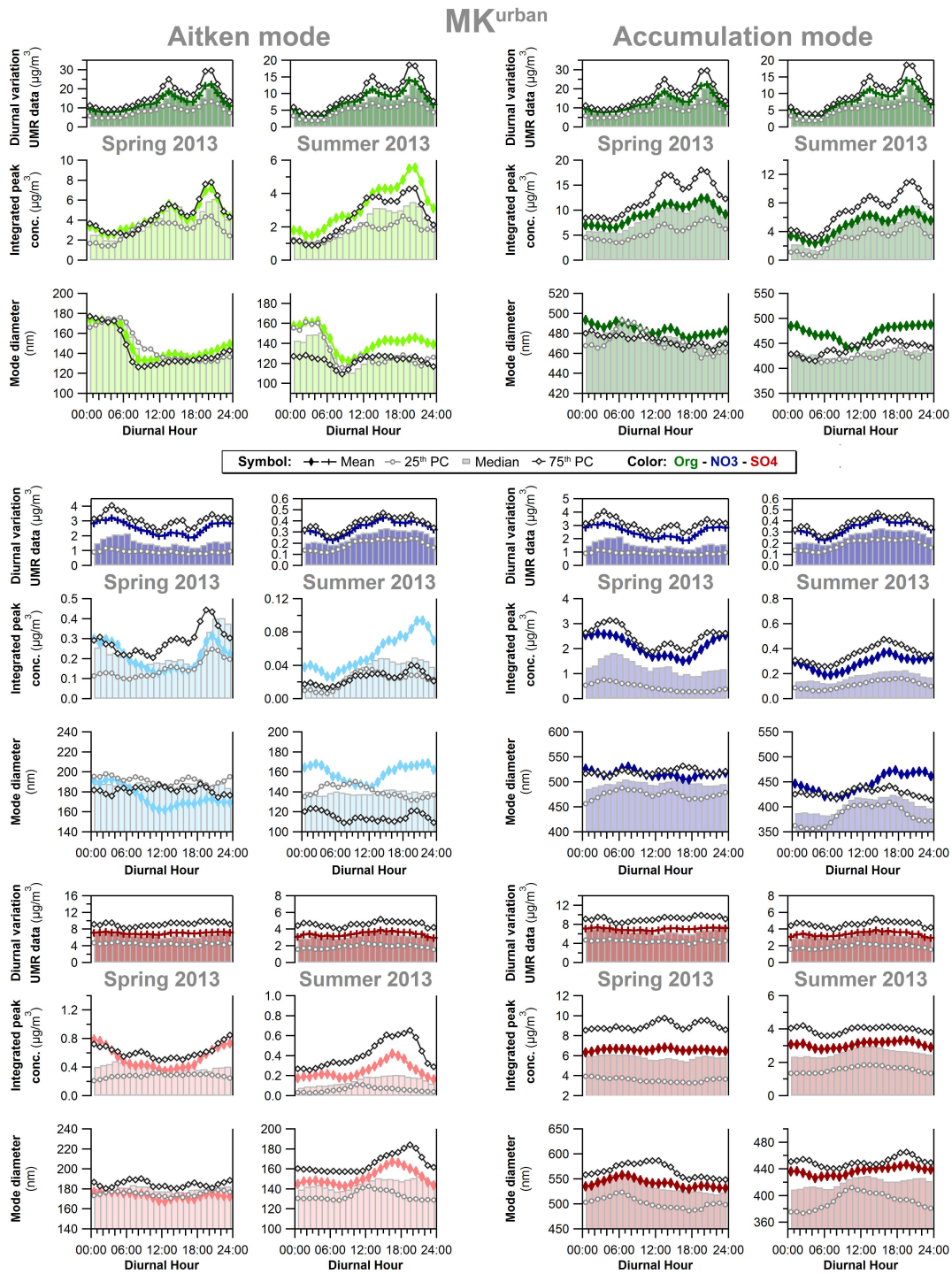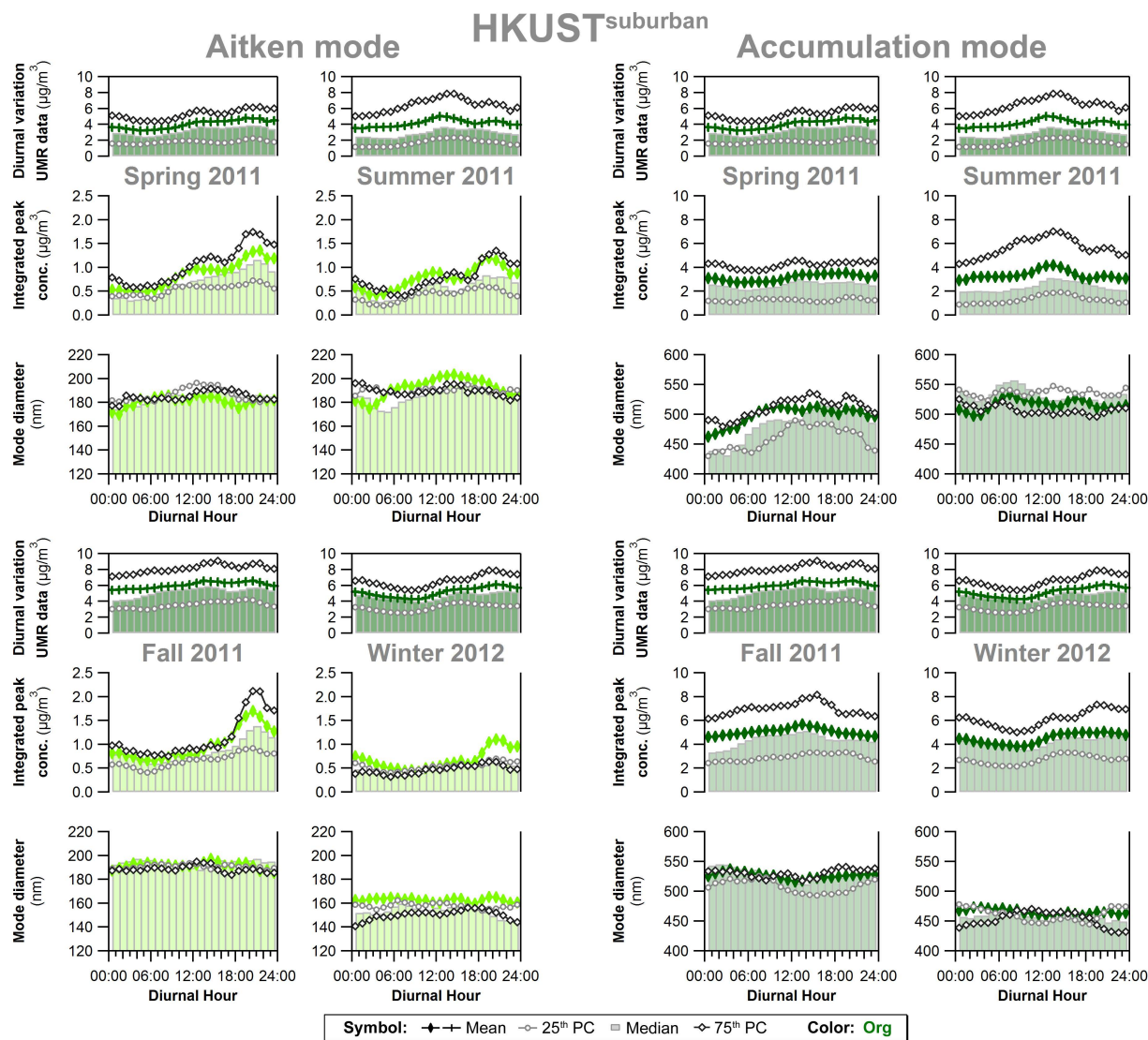
Figure D2. Mode diameter (mass median diameter - MMD), integrated particle mass concentration and width (geometric standard deviation - GSD) of the Aitken mode and accumulation mode from bimodal diurnal peak fits of organic, nitrate and sulfate size distributions at the Mong Kok urban site in spring 2013 and summer 2013; the top panel depicts the diurnal variations of total measured submicron organic, nitrate and sulfate concentrations (AMS V-mode data)

Figure D3. Mode diameter (mass median diameter - MMD), integrated particle mass concentration and width (geometric standard deviation - GSD) of the Aitken mode and accumulation mode from bimodal diurnal peak fits of organic size distributions at the suburban HKUST site in four seasons (May 2011- Feb 2012); the top panel depicts the diurnal variations of total measured submicron organic concentrations (AMS V-mode data)
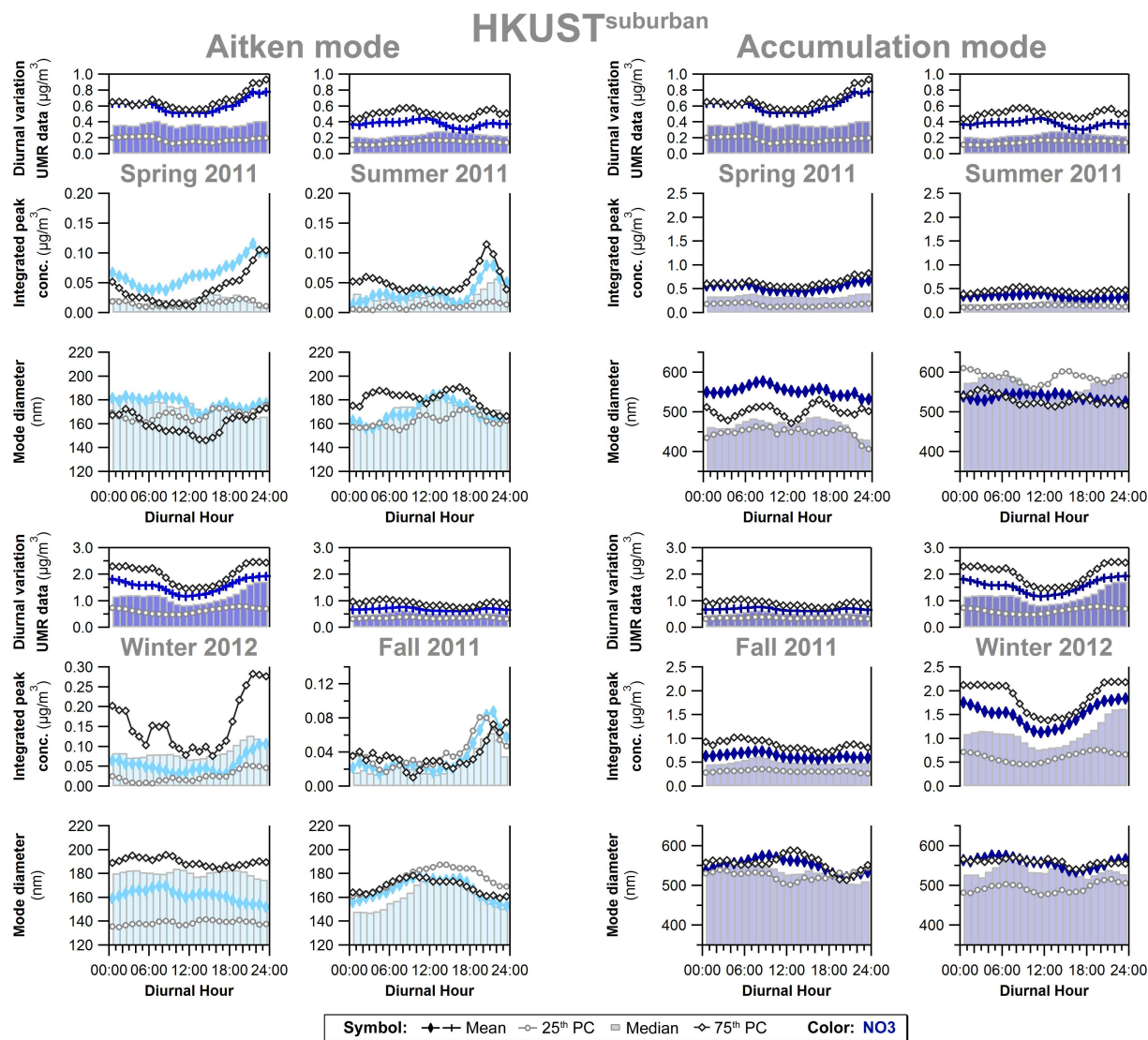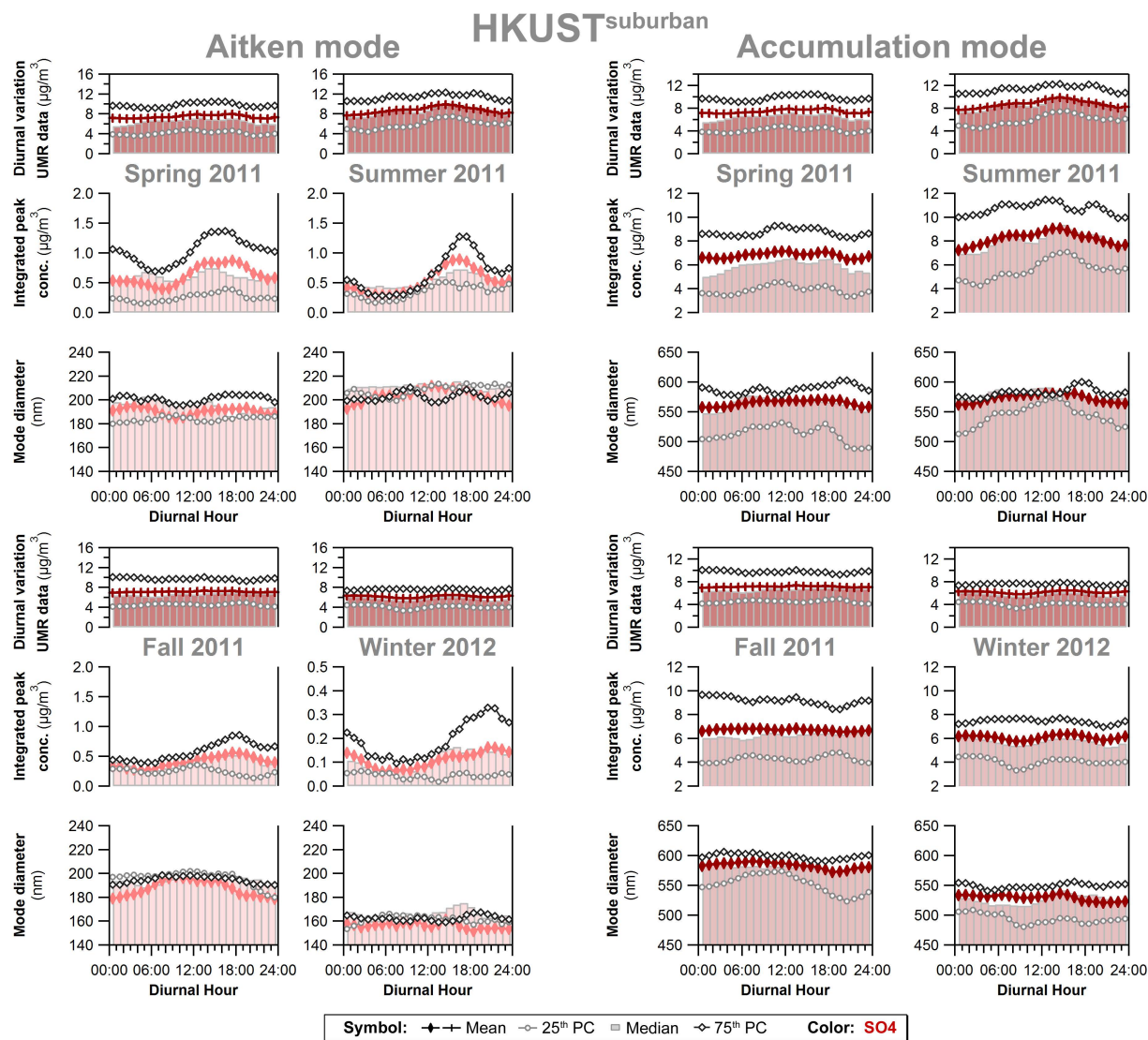
Figure D4. Mode diameter (mass median diameter - MMD), integrated particle mass concentration and width (geometric standard deviation - GSD) of the Aitken mode and accumulation mode from bimodal diurnal peak fits of nitrate size distributions at the suburban HKUST site in four seasons (May 2011- Feb 2012); the top panel depicts the diurnal variations of total measured submicron nitrate concentrations (AMS V-mode data)

Figure D5. Mode diameter (mass median diameter - MMD), integrated particle mass concentration and width (geometric standard deviation - GSD) of the Aitken mode and accumulation mode from bimodal diurnal peak fits of sulfate size distributions at the suburban HKUST site in four seasons (May 2011- Feb 2012); the top panel depicts the diurnal variations of total measured submicron sulfate concentrations (AMS V-mode data)
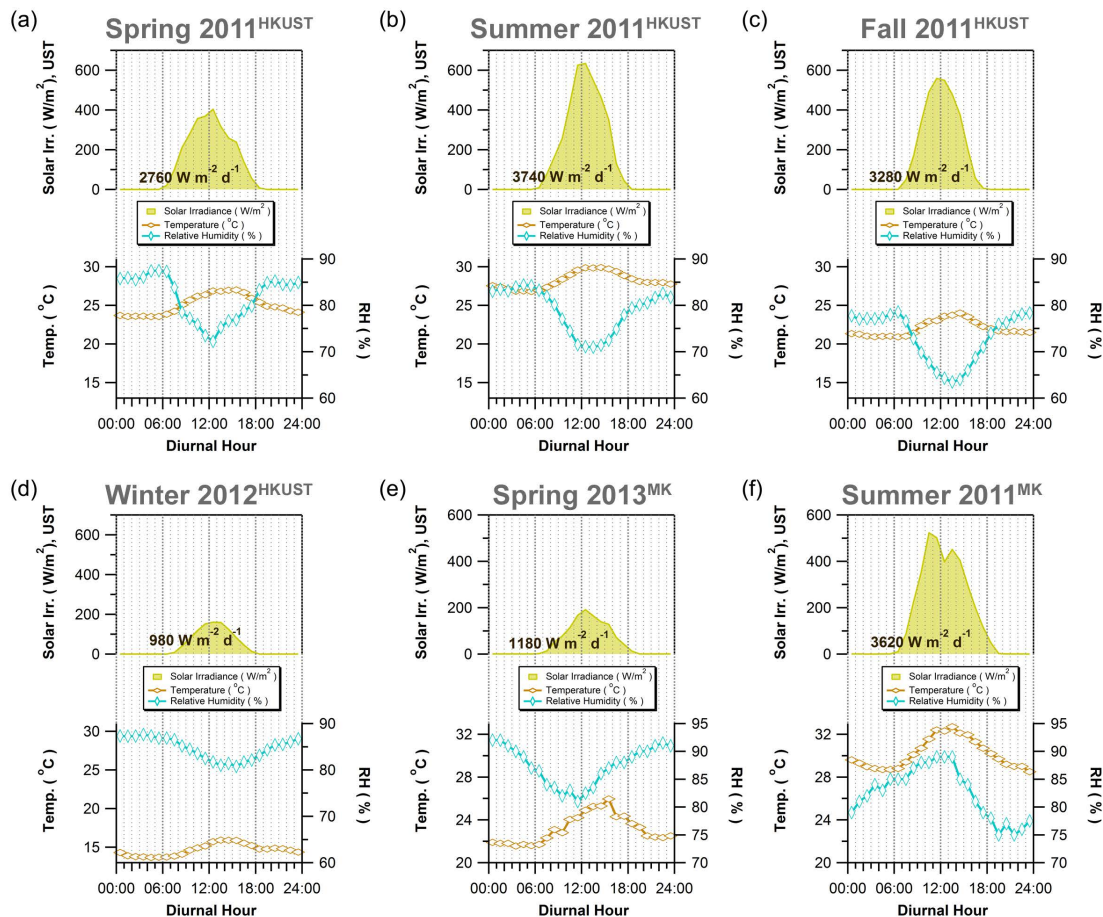
Figure D6. Diurnal variation of temperature (*orange*), RH (*blue*) and solar irradiance (*yellow*) in four seasons in 2011-2012 as well as spring and summer 2013; temperature and RH measurements from the HKUST supersite for the four seasons in 2011-2012, and from the Mong Kok urban site for spring and summer 2013; solar irradiance data always from the HKUST supersite.
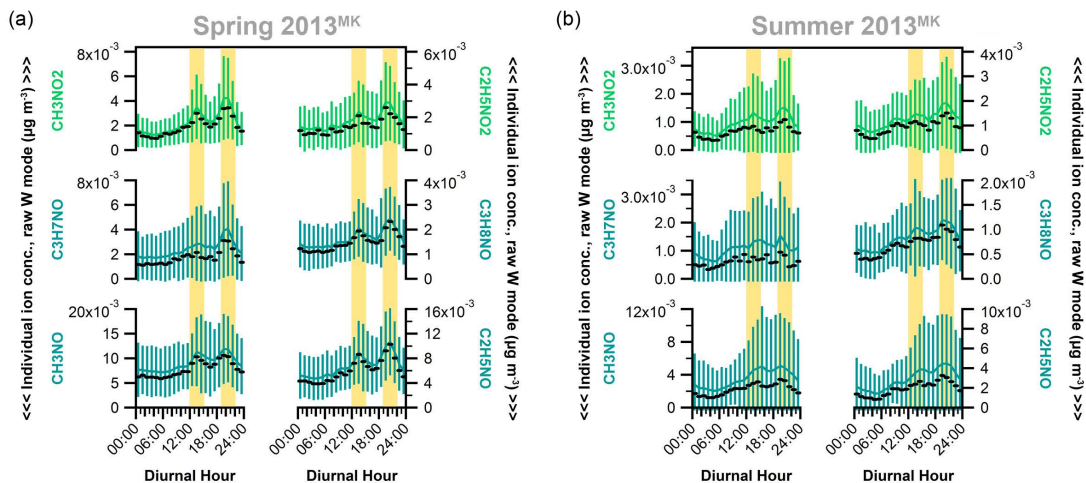

Figure D7. Diurnal variation of fitted $C_xH_yN_zO$ and $C_xH_yN_zO_2$ ions (*raw W-mode mass concentrations*) at the urban Mong Kok site in 2013 in spring (a) and summer (b), meal hours highlighted in yellow
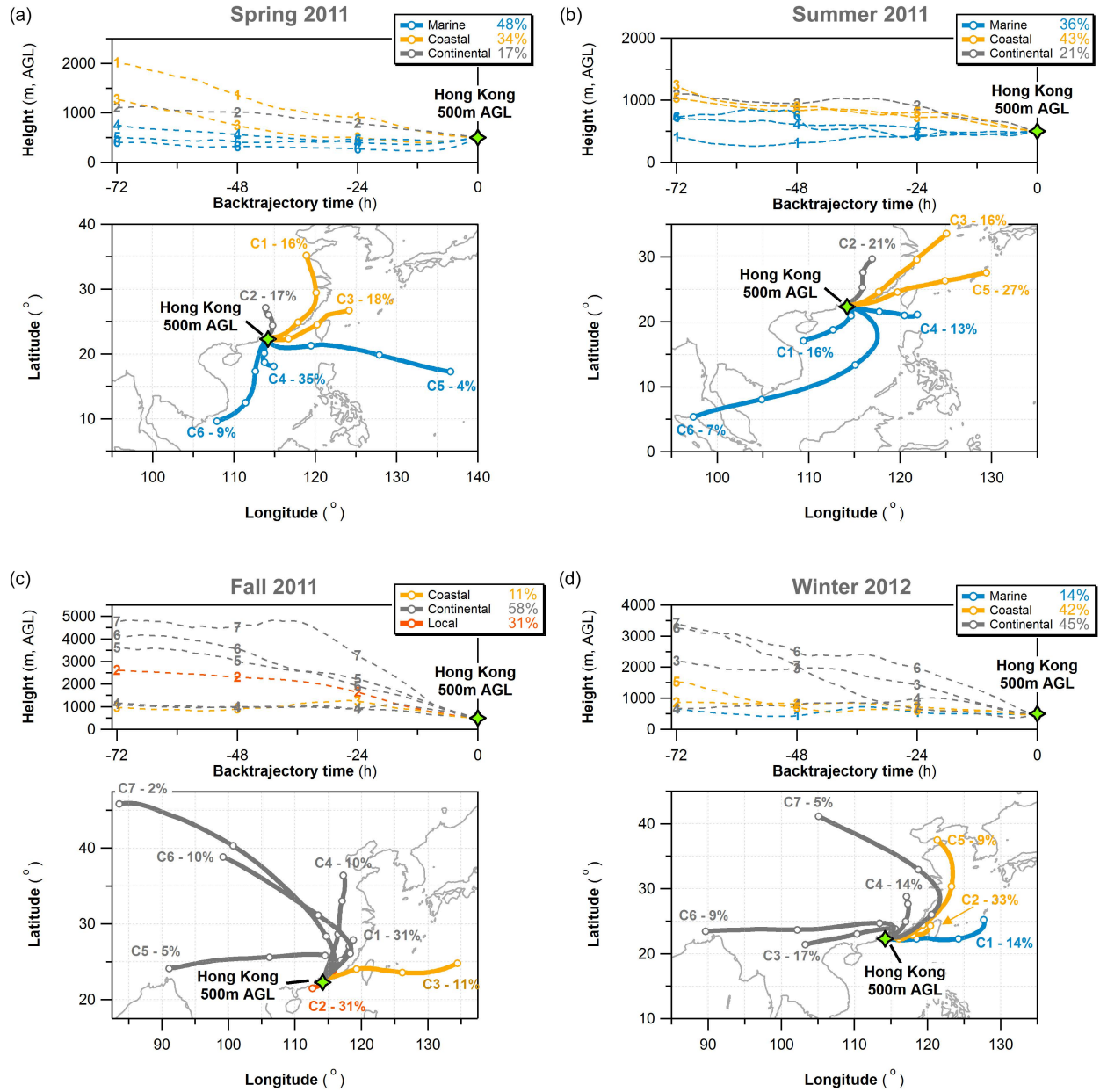
Figure D8. Means of clustered backtrajectories (HYSPLIT4, 72h backtrajectories) in each sampling season at the suburban HKUST site in (a) spring, (b) summer, (c) fall and (d) winter 2011-2012
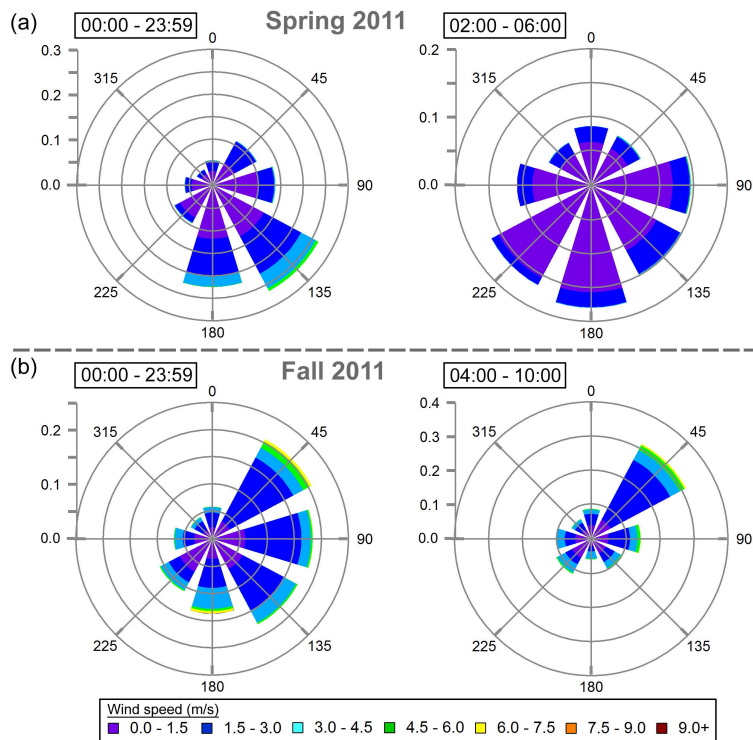
Figure D9. Wind rose plots for observed surface wind frequency at the suburban HKUST site in spring 2011 (2011-05) for the whole sampling period and the nighttime period between 02:00 and 06:00 (a) and in summer 2011 (2011-09) for the whole sampling period and the morning period between 04:00 and 10:00
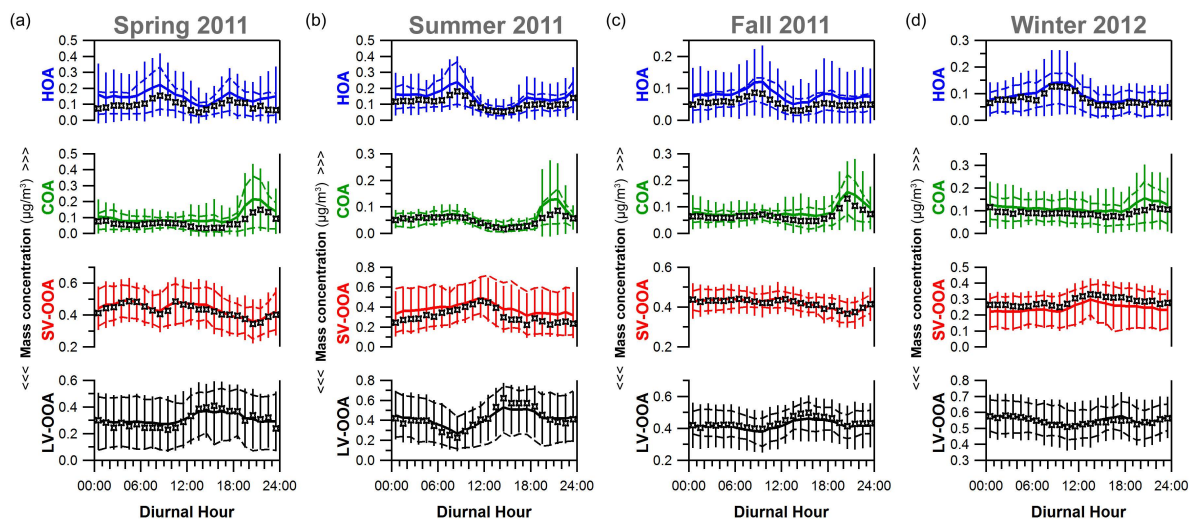

Figure D10. Diurnal variation of PMF-resolved organic aerosol factors at the suburban HKUST site in (a) spring, (b) summer, (c) fall and (d) winter 2011-2012, for details see Li et al. [*Li et al.*, 2015].
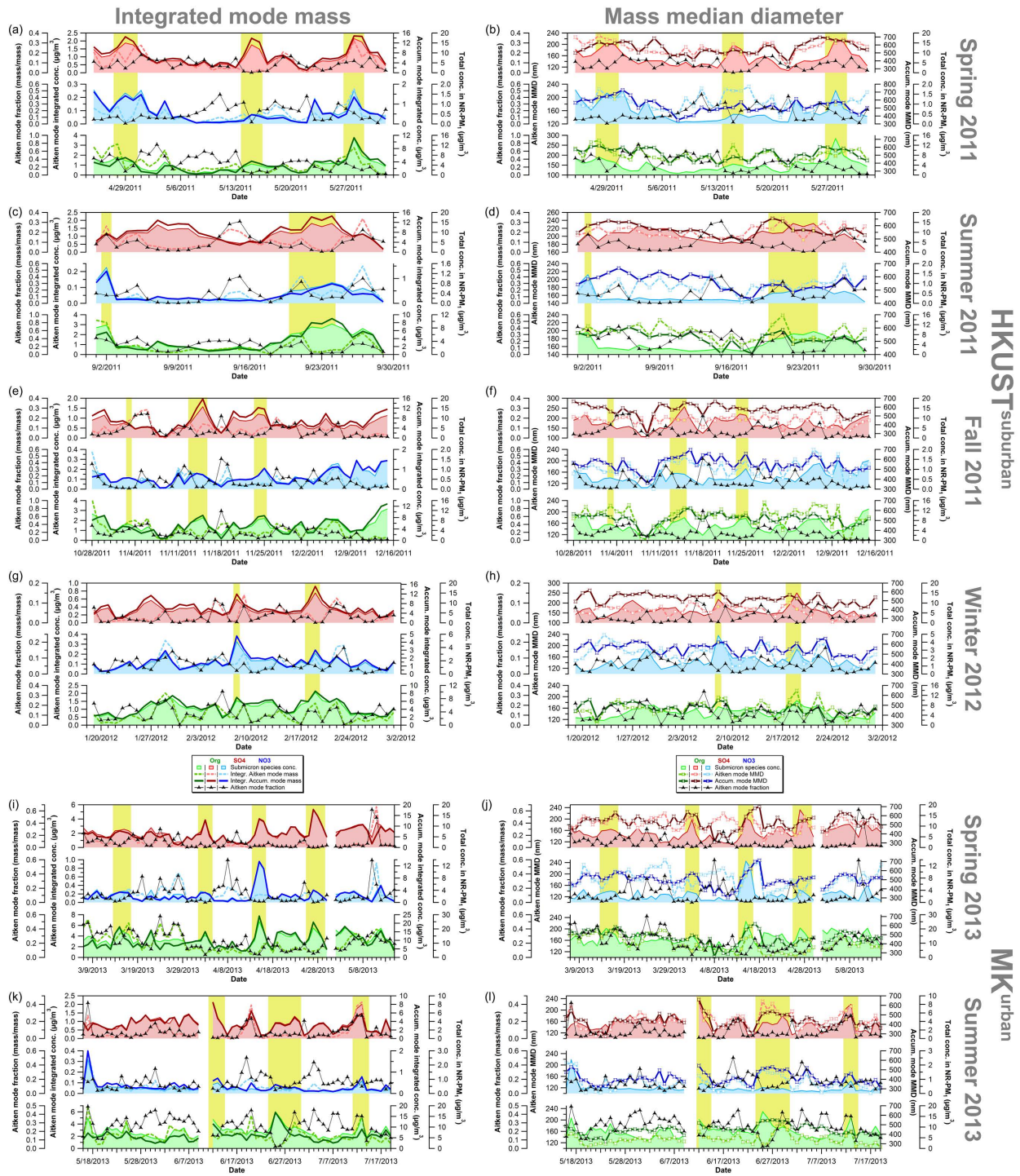
Figure D11. Time series of integrated particle mass concentrations (left-hand panels) and mass median diameters (right-hand panels) of Aitken and accumulation modes at the suburban HKUST supersite in four seasons in 2011-2012 (a-h) and the urban Mong Kok site in 2013 (i-l), total species mass concentrations are based on V-mode measurements.
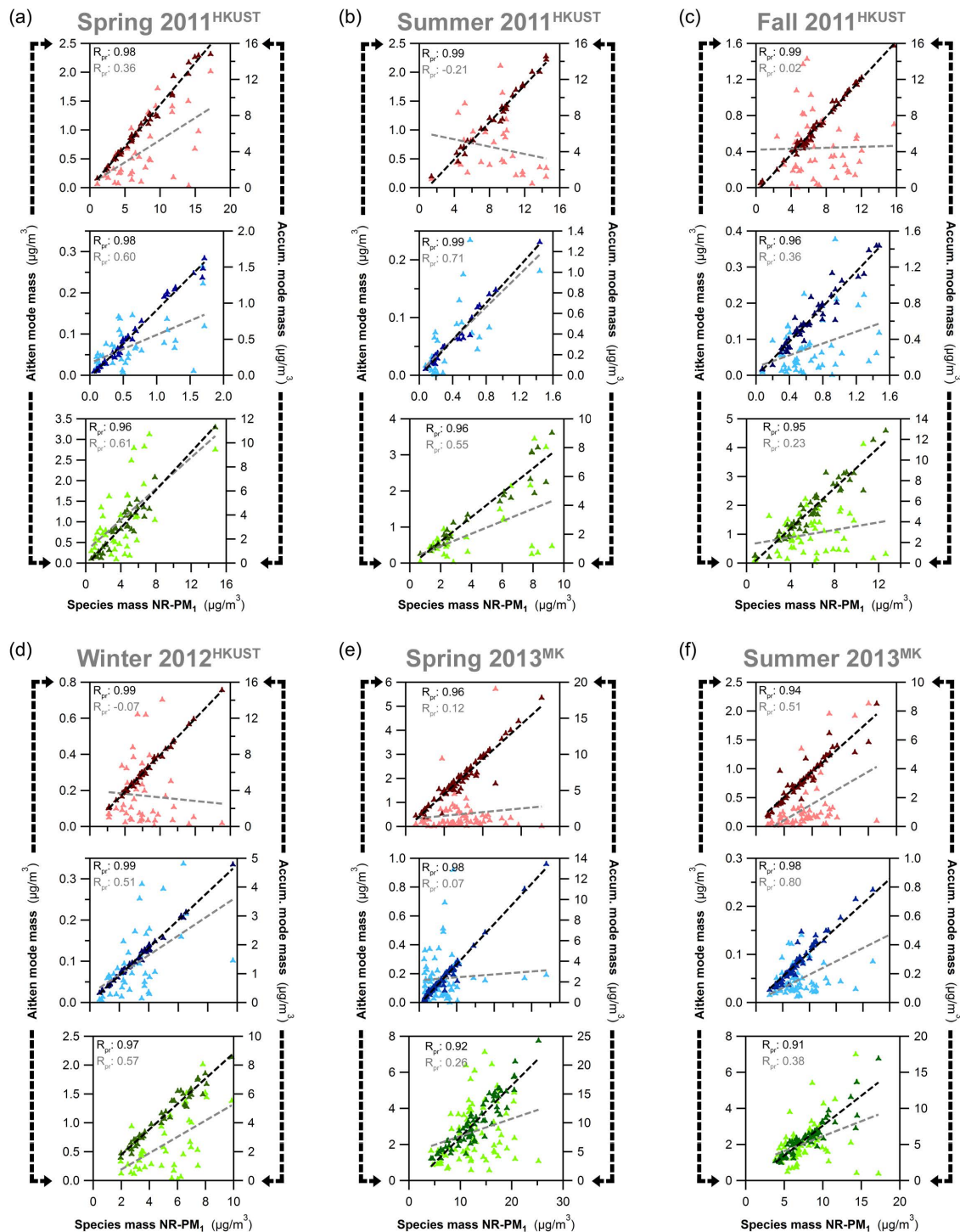
Figure D12. Scatter plot of Aitken and accumulation mode mass concentrations and total species concentrations in NR-PM$_1$ (V-mode at the HKUST supersite (a-d) and the Mong Kok urban site (e-f)

References

Canagaratna, M. R., et al. (2007), Chemical and microphysical characterization of ambient aerosols with the aerodyne aerosol mass spectrometer, *Mass Spectrometry Reviews*, *26*(2), 185-222.

DeCarlo, P. F., J. G. Slowik, D. R. Worsnop, P. Davidovits, and J. L. Jimenez (2004), Particle morphology and density characterization by combined mobility and aerodynamic diameter measurements. Part 1: Theory, *Aerosol Science and Technology*, *38*(12), 1185-1205.

DeCarlo, P. F., et al. (2006), Field-deployable, high-resolution, time-of-flight aerosol mass spectrometer, *Analytical Chemistry*, *78*(24), 8281-8289.

Drewnick, F., et al. (2005), A new time-of-flight aerosol mass spectrometer (TOF-AMS) - Instrument description and first field deployment, *Aerosol Science and Technology*, *39*, 637-658.

Jayne, J. T., D. C. Leard, X. F. Zhang, P. Davidovits, K. A. Smith, C. E. Kolb, and D. R. Worsnop (2000), Development of an aerosol mass spectrometer for size and composition analysis of submicron particles, *Aerosol Science and Technology*, *33*(1-2), 49-70.

Jimenez, J. L., et al. (2003), Ambient aerosol sampling using the Aerodyne Aerosol Mass Spectrometer, *J. Geophys. Res.*, *108*(D7), 8425.

Jimenez, J. L., et al. (2007), Development and application of a high-resolution time-of-flight aerosol mass spectrometer, *Abstracts of Papers of the American Chemical Society*, *233*, 590-590.

Lee, B. P., Y. J. Li, J. Z. Yu, P. K. K. Louie, and C. K. Chan (2015), Characteristics of submicron particulate matter at the urban roadside in downtown Hong Kong—Overview of 4 months of continuous high-resolution aerosol mass spectrometer measurements, *Journal of Geophysical Research: Atmospheres*, *120*(14), 7040-7058.

Li, Y. J., B. P. Lee, L. Su, J. C. H. Fung, and C. K. Chan (2015), Seasonal characteristics of fine particulate matter (PM) based on high resolution time-of-flight aerosol mass spectrometric (HR-ToF-AMS) measurements at the HKUST Supersite in Hong Kong, *Atmos. Chem. Phys.*, *15*(15), 37-53.

Slowik, J. G., K. Stainken, P. Davidovits, L. R. Williams, J. T. Jayne, C. E. Kolb, D. R. Worsnop, Y. Rudich, P. F. DeCarlo, and J. L. Jimenez (2004), Particle morphology and density characterization by combined mobility and aerodynamic diameter measurements. Part 2: Application to combustion-generated soot aerosols as a function of fuel equivalence ratio, *Aerosol Science and Technology*, *38*(12), 1206-1222.